The Astrophysical Journal, 737:101 (14pp), 2011 August 20 doi:10.1088/0004-637X/737/2/101

ACTIVE GALACTIC NUCLEUS PAIRS FROM THE SLOAN DIGITAL SKY SURVEY. I. THE FREQUENCY ON ∼5–100 kpc SCALES

Xin Liu[1,2,4], Yue Shen[1], Michael A. Strauss[2], and Lei Hao[3]
[1] Harvard-Smithsonian Center for Astrophysics, 60 Garden Street, Cambridge, MA 02138, USA
[2] Department of Astrophysical Sciences, Princeton University, Peyton Hall-Ivy Lane, Princeton, NJ 08544, USA
[3] Shanghai Astronomical Observatory, Chinese Academy of Sciences, 80 Nandan Road, Shanghai 200030, China
Received 2011 March 16; accepted 2011 June 23; published 2011 August 8

ABSTRACT

Galaxy–galaxy mergers and close interactions have long been regarded as a viable mechanism for channeling gas toward the central supermassive black holes (SMBHs) of galaxies which are triggered as active galactic nuclei (AGNs). AGN pairs, in which the central SMBHs of a galaxy merger are both active, are expected to be common from such events. We conduct a systematic study of 1286 AGN pairs at $\bar{z} \sim 0.1$ with line-of-sight velocity offsets $\Delta v < 600$ km s^{-1} and projected separations $r_p < 100\,h_{70}^{-1}$ kpc, selected from the Seventh Data Release of the Sloan Digital Sky Survey (SDSS). This AGN pair sample was drawn from 138,070 AGNs optically identified based on diagnostic emission line ratios and/or line widths. The fraction of AGN pairs with $5\,h_{70}^{-1}$ kpc $\lesssim r_p < 100\,h_{70}^{-1}$ kpc among all spectroscopically selected AGNs at $0.02 < z < 0.16$ is 3.6% after correcting for SDSS spectroscopic incompleteness; ∼30% of these pairs show morphological tidal features in their SDSS images, and the fraction becomes ≳80% for pairs with the brightest nuclei. Our sample increases the number of known AGN pairs on these scales by more than an order of magnitude. We study their AGN and host-galaxy star formation properties in a companion paper.

Key words: black hole physics – galaxies: active – galaxies: interactions – galaxies: nuclei – quasars: general

Online-only material: color figures, machine-readable table

1. INTRODUCTION

Binary supermassive black holes (SMBHs) are thought to be a generic outcome of galaxy–galaxy mergers in the hierarchical paradigm of structure formation (Begelman et al. 1980; Milosavljević & Merritt 2001; Yu 2002), given that most massive galaxies harbor central SMBHs (Kormendy & Richstone 1995; Richstone et al. 1998). If both SMBHs accrete material during the same stage of a galaxy–galaxy merger, they can be identified as a pair of active galactic nuclei (AGNs). However, it is difficult to predict from first principles when one and in particular both SMBHs become active during a merger (e.g., Shlosman et al. 1990; Armitage & Natarajan 2002; Wada 2004; Dotti et al. 2007). The frequency of AGN pairs can constrain models involving galaxy merger rates and tidally triggered AGN activity (Yu et al. 2011). Their host-galaxy properties may offer clues to the external and internal conditions under which both SMBHs can be activated during galaxy–galaxy tidal encounters.

When two galaxies merge, the two SMBHs in-spiral, form a bound binary, and harden, before they finally coalesce (Begelman et al. 1980). The coalescence of binary SMBHs is expected to be the strongest source of gravitational waves in the universe, the detection of which would directly test general relativity and could probe SMBH populations out to the early universe (Thorne 1987; Haehnelt 1994; Holz & Hughes 2005). However, there is still little direct observational evidence for small-separation (≲10 pc) gravitationally bound binary SMBHs on Keplerian orbits (see, e.g., the review of Colpi & Dotti 2009). 0402+379 is the only unambiguous case known. This object was detected by Very Long Baseline Interferometry as a pair of flat-spectrum radio point sources with a projected separation of ∼7 pc (Rodriguez et al. 2006; Valtonen et al. 2008). At the early stages of a merger, large-separation (kpc to tens of kpc) AGN pairs where the galactic potential dominates can readily be spatially resolved at cosmological distances. They provide boundary/initial conditions for small-separation pairs. By characterizing the large-separation population, we may gain indirect but useful information on the small-separation population.

There are an increasing number of examples of interacting AGN pairs with kpc to tens-of-kpc separations. Such objects have been identified in the X-ray (e.g., Komossa et al. 2003; Ballo et al. 2004; Bianchi et al. 2008; Piconcelli et al. 2010; Mazzarella et al. 2011) the radio (e.g., Owen et al. 1985), or the optical (e.g., Barth et al. 2008; Comerford et al. 2009b; Green et al. 2010; Liu et al. 2010a) regimes. However, most of the known cases of kpc-scale AGN pairs have been serendipitous discoveries. To systematically identify and characterize the population of AGN pairs, we selected 167 obscured AGNs with double-peaked narrow emission lines from a parent sample of 14,756 AGNs (Liu et al. 2010b) in the Sloan Digital Sky Survey (SDSS; York et al. 2000). Using higher resolution near-IR imaging and spatially resolved optical spectroscopy, we identified four kpc-scale AGN pairs among 43 of the 167 double-peaked AGNs (Liu et al. 2010a; Shen et al. 2010b). While our work has demonstrated that the double-peak approach allows us to systematically identify kpc-scale AGN pairs, it has two inherent limitations. First, the approach is biased against pairs with line-of-sight (LOS) velocities smaller than ∼150 km s^{-1} due to the limited spectral resolution of SDSS spectra. Second, it is biased against pairs with separations ≳ a few kpc because pairs with projected separations larger than 3″ (the diameter of the SDSS fiber) will not fall within a single SDSS fiber.

To circumvent the limitations of the double-peak method and to build up the sample of AGN pairs along the merger sequence, we take a complementary approach to identify them. We start with a sample of spectroscopically identified AGNs and select physical pairs with special attention paid to those that are in mergers or close interactions. Because each AGN in a pair has

[4] Einstein Fellow.

a separate SDSS spectrum, the current approach is not limited by the SDSS spectral resolution or by the 3″ fiber size. The current sample is sensitive to an earlier stage, with separations of a few kpc to tens of kpc, of galaxy–galaxy mergers than is the double-peak approach. Such systems are quite scarce, so a statistically meaningful study requires homogeneous and large-area redshift surveys such as the SDSS. While galaxy pairs with projected angular separations smaller than 55″ cannot both be observed spectroscopically on the same SDSS plate due to the finite diameter of the fibers, those in the overlap regions of adjacent plates can both be spectroscopically observed (Strauss et al. 2002; Blanton et al. 2003).

The present paper is the first in a series in which we present a statistical sample of AGN pairs from the Seventh Data Release (DR7; Abazajian et al. 2009) of the SDSS. In Section 2, we describe sample selection, and discuss incompleteness and selection biases. We address the frequency of AGN pairs among the parent sample of optically identified AGNs in Section 3. We discuss the implications of our results in Section 4 and conclude in Section 5. In a companion paper (Liu et al. 2011a, hereafter Paper II), we will characterize host-galaxy recent star formation and BH accretion properties of the AGN pair sample presented here. Throughout we assume a ΛCDM (Λ-cold dark matter) cosmology with $\Omega_m = 0.3$, $\Omega_\Lambda = 0.7$, and $H_0 = 70\ h_{70}$ km s^{-1} Mpc^{-1}.

2. SAMPLE SELECTION

In this section, we describe our approach to select AGN pairs. In Section 2.1, we construct a parent AGN sample optically identified from the spectroscopic sample of SDSS DR7. We then draw AGN pairs with LOS velocity offsets $\Delta v < 600$ km s^{-1} and projected separations $r_p < 100\,h_{70}^{-1}$ kpc (Section 2.2). To mitigate contamination due to pairs that are closely separated but are not interacting and to focus on AGN pairs that are unambiguously experiencing strong tidal encounters, we visually inspect the SDSS images of all AGN pairs and further identify a subset, which we call the "tidal" sample, that exhibits unambiguous morphological tidal features (Section 2.3). We discuss our sample completeness and selection biases in Section 2.4.

2.1. The Parent AGN Sample

Our parent AGN sample includes objects drawn from the SDSS "narrow-line"[5] AGN sample (Kauffmann et al. 2003a), broad-line AGNs (Hao et al. 2005a, 2005b), narrow-line quasars (Zakamska et al. 2003; Reyes et al. 2008), and broad-line quasars (Schneider et al. 2010), all from the DR7.[6] Below we describe the selection criteria for each population. The redshift cut for all objects is $0.02 < z < 0.33$. The lower redshift limit is to balance the need to include nearby galaxies and to avoid redshifts where peculiar velocities can cause substantial deviations from Hubble flow; the upper redshift limit is to ensure Hα coverage in the SDSS spectra for AGN identification.

1. Narrow-line AGNs. First, we select AGNs from the MPA-JHU SDSS DR7 galaxy catalog[7] (see Aihara et al. 2011, for a description of the catalog) drawn from the SDSS DR7 spectroscopic database; this database includes 869,580 targets[8] spectrally classified as galaxies by the specBS pipeline (Adelman-McCarthy et al. 2008; Aihara et al. 2011; see also a discussion in Blanton et al. 2005) or quasars that are targeted as galaxies (Strauss et al. 2002; Eisenstein et al. 2001) and have redshifts $z < 0.7$. We adopt redshifts z and stellar velocity dispersions σ_* from the specBS pipeline. Additional spectroscopic and photometric properties such as emission-line fluxes and stellar masses are taken from the MPA-JHU data product. The emission line measurements are from Gaussian fits to continuum-subtracted spectra (Brinchmann et al. 2004; Tremonti et al. 2004). The MPA-JHU emission-line fluxes have been normalized to SDSS r-band photometric fiber magnitude and have been corrected for Galactic foreground extinction following O'Donnell (1994) using the map of Schlegel et al. (1998). The stellar mass estimates are total stellar masses derived from population synthesis fits using the Bruzual & Charlot (2003) models to SDSS broadband photometry (Kauffmann et al. 2003b; Salim et al. 2007).
We have two selection criteria: (1) emission lines Hβ, [O III] λ5007, Hα, and [N II] λ6584 must all be detected with signal-to-noise ratios (S/N) > 3, and (2) the diagnostic emission-line ratios [O III] λ5007/Hβ and [N II] λ6584/Hα suggest that the dominant excitation mechanism is from AGNs rather than stellar photo-ionization (Baldwin et al. 1981; Osterbrock & Pogge 1985; Veilleux & Osterbrock 1987) according to the empirical criterion,

$$\log([\mathrm{O\,III}]/\mathrm{H}\beta) > \frac{0.61}{\log([\mathrm{N\,II}]/\mathrm{H}\alpha) - 0.05} + 1.3, \quad (1)$$

as suggested by Kauffmann et al. (2003a). We address the effect of the adopted S/N threshold for emission-line detections on our results in Section 3. 129,277 objects meet these two criteria. The Kauffmann et al. (2003a) empirical criterion includes AGN-H II "composite" objects, which represent over half the sample. If we were to adopt instead the theoretical "starburst limit" suggested by Kewley et al. (2001),

$$\log([\mathrm{O\,III}]/\mathrm{H}\beta) > \frac{0.61}{\log([\mathrm{N\,II}]/\mathrm{H}\alpha) - 0.47} + 1.19, \quad (2)$$

in order to exclude the AGN–H II composites, the sample would be reduced to 50,624 objects. We include composites in our analysis, because the results would be otherwise biased against starburst-dominated systems with moderate AGN activity. In a study of hard X-ray selected moderate-luminosity AGNs at $z < 0.05$ from the *Swift* Burst Alert Telescope AGN sample (Tueller et al. 2010), Koss et al. (2010) find that 33% of AGNs in merging systems show composite or star-forming diagnostic lines. Similarly, Goulding & Alexander (2009) found evidence of star formation in the optical emission lines of AGNs identified based on *Spitzer* infrared spectra of IR luminous galaxies.
2. Narrow-line quasars. Second, we supplement the parent sample with 112 objects from the narrow-line quasar sample of Reyes et al. (2008). These objects satisfy our selection criteria for narrow-line AGNs but are not already

[5] The "narrow-line" classification here is not meant to be strict. Some AGNs in this sample show broad-line components as well (e.g., Hao et al. 2005b).
[6] The narrow-line quasar sample of Reyes et al. (2008) was selected from a sample corresponding to ∼80% of the Data Release 6 (DR6) spectroscopic database (Adelman-McCarthy et al. 2008) so we may miss a small number of narrow-line quasars post DR6.
[7] www.mpa-garching.mpg.de/SDSS/DR7/
[8] Here and throughout, we quote the numbers of unique galaxies after excluding duplicate observations of the same galaxy.

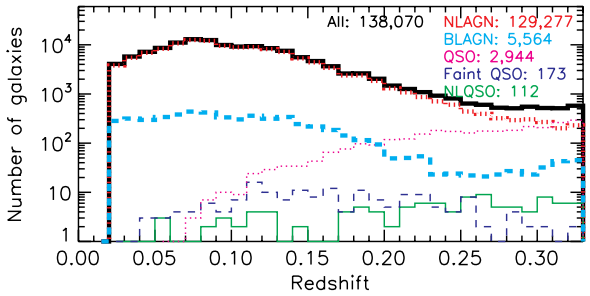

Figure 1. Redshift distributions of the parent AGN sample (black solid curve) and the subsamples it contains (color curves). We use "NLAGN" to denote narrow-line AGNs according to the Kauffmann et al. (2003a) criterion, "BLAGN" for broad-line AGNs according to the Hao et al. (2005b) classification that are not contained in the MPA-JHU DR7 AGN catalog, "NLQSO" for narrow-line quasars in the Reyes et al. (2008) sample but not in the MPA-JHU DR7 AGN catalog, "QSO" for quasars in the catalog of Schneider et al. (2010), and "Faint QSO" for quasars above the flux limit of the SDSS main galaxy sample but whose luminosities are too low to be included in the Schneider et al. (2010) catalog. Refer to Section 2 for details.

(A color version of this figure is available in the online journal.)

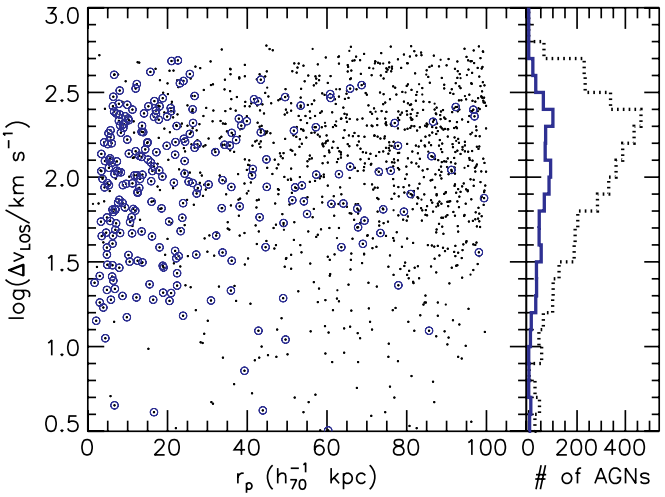

Figure 2. Projected separation r_p vs. LOS velocity offset Δv (on a logarithmic scale) for AGN pairs (black dots and dotted histogram) and the subset with identified morphological tidal features (blue open circles and solid histogram). The Δv distributions have been corrected for spectroscopic incompleteness (Section 2.2.1). We caution that values below $\Delta v = 30$ km s^{-1} are dominated by redshift measurement uncertainties.

(A color version of this figure is available in the online journal.)

contained in the MPA-JHU SDSS DR7 galaxy catalog because they were not part of the main spectroscopic galaxy sample.

3. Broad-line AGNs. Third, we supplement the sample with broad-line AGNs selected by Hao et al. (2005b) extended to SDSS DR7. These are objects selected from the SDSS main galaxy sample (Strauss et al. 2002) at $z < 0.33$ which have a broad Hα component (full width at half maximum (FWHM) >1200 km s^{-1}) from multi-Gaussian fits with a rest-frame Hα equivalent width (EW) >3 Å. There are 9573 such objects at $0.02 < z < 0.33$, and 3710 of them are included in the MPA-JHU DR7 AGN catalog or in the SDSS DR7 quasar catalog (see below). Hao et al. (2005b) show that the narrow-line components of most broad-line AGNs satisfy the Kewley et al. (2001) criteria for narrow-line AGNs. Given the purpose of this work, we supplement the parent AGNs with the new 5863 broad-line AGNs, and keep the 3710 overlaps in our "narrow-line" AGN category without labeling them more carefully. As shown by Reyes et al. (2008), it can be unclear whether an AGN is a narrow-line or a broad-line object when the broad component is relatively faint or when the forbidden emission lines have non-Gaussian profiles (such as extended wings and/or double peaks). The classification can be further complicated by the presence of scattered broad-line region light in obscured quasars (e.g., Zakamska et al. 2006; Liu et al. 2009).
4. Broad-line quasars. We next supplement the parent AGNs with 2944 objects at $0.02 < z < 0.33$ from the SDSS DR7 quasar catalog (Schneider et al. 2010). The SDSS quasar catalog of Schneider et al. (2010) has a luminosity cut $M_i < -22.0$ mag. There are quasars whose luminosities are too low to be included in the Schneider et al. (2010) quasar catalog but have extinction-corrected Petrosian $14.5 < r < 17.77$ mag consistent with the flux limit of the SDSS main galaxy sample (Strauss et al. 2002). To include those as well we searched through all objects targeted as "quasars" (Richards et al. 2002) at $0.02 < z < 0.33$ in the spectroscopic sample of SDSS DR7 and further supplemented the sample with 173 broad-line objects after rejecting stellar contaminants. These quasars are not included in the DR7 version of the broad-line AGN sample as they were not targeted as "galaxies" (Richards et al. 2002).

The resulting parent AGN sample consists of 138,070 optically selected AGNs at $0.02 < z < 0.33$. We list the numbers of galaxies in each selection category in Table 2. Among the parent AGN sample, 94% are included in the MPA-JHU DR7 galaxy catalog, 2.9% of which are classified as broad-line AGNs according to Hao et al. (2005b) because they have weak FWHM > 1200 km s^{-1} Hα components. This catalog serves as the starting point from which we draw the "pair" sample based on projected and radial separation criteria, and a subset which shows tidal features in SDSS images. To put our results on AGN pairs into context and to compare with "ordinary" AGNs, we also draw control AGNs from this parent sample (Paper II). Figure 1 shows the redshift distribution of the parent AGN sample and its sub-populations.

2.2. AGN Pairs

We select AGN pairs from our parent sample of AGNs based on the following criteria: (1) projected separation $r_p < 100\,h_{70}^{-1}$ kpc and (2) LOS velocity difference $\Delta v < 600$ km s^{-1}. We choose 100 kpc to minimize contamination due to pairs that are closely separated but are not interacting while maintaining a large dynamical range in separation. 100 kpc is somewhat larger than the typical threshold values adopted in galaxy pair studies (e.g., Barton et al. 2000; Ellison et al. 2008; Darg et al. 2010). The velocity-offset threshold also balances contamination and statistics; it is comparable to the galaxy pairwise velocity dispersion for projected separations $0.15 \leqslant r_p \leqslant 5\,h_{70}^{-1}$ Mpc (e.g., Zehavi et al. 2002). While galaxy pairs with small projected separations and small velocity offsets are likely to be bound and merge within a Hubble time, the maximum velocity offset of an interacting galaxy pair depends on local environment. To check whether we missed a significant population of interacting galaxies with even larger velocity offsets, we show the distribution of Δv of the AGN pairs in Figure 2. The distribution function drops sharply at $\Delta v \gtrsim 300$ km s^{-1} and the threshold value 600 km s^{-1} is on the tail of the distribution, verifying that the Δv threshold is adequate.

Figure 3. SDSS *gri*-color composite images (Lupton et al. 2004) of six examples of AGN multiples. The top row displays three systems of AGN triples, whereas the bottom row presents two quadruples and a quintuple. Red circles indicate the locations of AGNs. North is up and east is to the left. The field of view (FOV) of each panel is $100'' \times 100''$. See Table 1 for coordinates, redshift, and other photometric and spectroscopic measurements of each AGN.

(A color version of this figure is available in the online journal.)

We visually inspected the SDSS images of all spectroscopically selected pairs and rejected 34 false positives due to multiple spectroscopic observations of different locations of the same galaxy. The final AGN pair sample includes 1286 systems with 1244 doubles, 39 triples, two quadruples, and one quintuple totalling 2616 AGNs. Figure 3 shows the SDSS images of six examples of AGN multiples, although they all have large separations without obvious tidal features. Using spatially resolved spectroscopic follow-up of AGN pairs in the sample with $r_p < 10\,h_{70}^{-1}$ kpc and having a third close companion, Liu et al. (2011b) discover a kpc-scale triple AGN. In Table 1, we list basic photometric and spectroscopic measurements for all 1286 systems of AGN pairs or multiples. Figure 4 shows their distributions of redshift and projected separations. While the parent sample spans a redshift range of $0.02 < z < 0.33$, only 24 pairs are found at $z > 0.16$ mainly reflecting the sparseness of the parent AGN sample. To mitigate uncertainties due to small number statistics at the higher redshift end, we restrict our statistical analysis to the 2568 AGNs at $z < 0.16$.

We show in Figure 5 the optical diagnostic line ratios [O III] λ5007/Hβ and [N II] λ6584/Hα of AGNs in the pair sample that are contained in the MPA-JHU SDSS DR7 galaxy catalog. Sixty-three percent of AGNs in the pair sample lie above the theoretical "starburst limit" of Kewley et al. (2001). In Paper II, we will use this sample to examine star formation and accretion properties in the host galaxies of AGN pairs and their correlations with pair separation.

2.2.1. Correction for SDSS Spectroscopic Incompleteness

Our sample of AGN pairs is incomplete for pairs with projected angular separations smaller than 55″ because both galaxies are required to have SDSS spectroscopic observations. Due to the finite size of the SDSS fibers, galaxy pairs with separations smaller than 55″ will not both be observed unless they fall in the overlap regions on adjacent plates (Strauss et al.

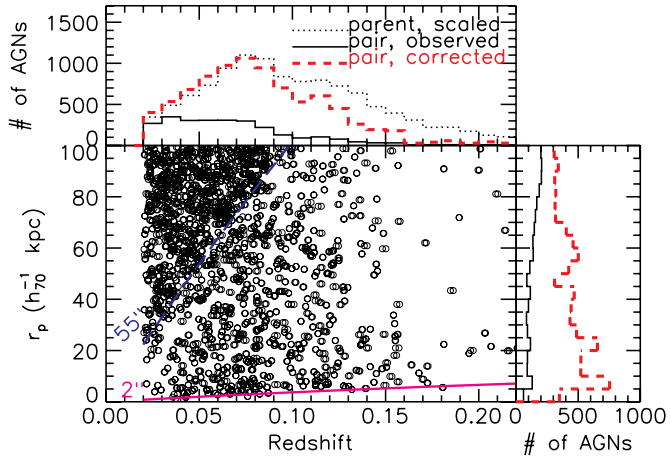

Figure 4. Redshift vs. projected separation (r_p) for objects in AGN pairs. The blue dashed curve marks the separation of 55″, below which the observed pair sample is incomplete due to SDSS fiber collision (Section 2.2.1). The black solid histograms show the observed redshift and r_p distributions of AGN pairs, whereas the red dashed histograms represent the distribution after correction for SDSS spectroscopic incompleteness. The dotted histogram is the redshift distribution of the parent AGN sample scaled down by an arbitrary factor for display purposes. The magenta solid curve denotes the separation of 2″, below which the observed pair sample is incomplete because smaller separation pairs are not resolved by SDSS imaging (Abazajian et al. 2009).

(A color version of this figure is available in the online journal.)

Table 1
SDSS AGN Pairs

SDSS Designation (1)	Plate (2)	Fiber (3)	MJD (4)	Redshift (5)	$\Delta\theta$ ($''$) (6)	r_p (h_{70}^{-1} kpc) (7)	Δv (km s^{-1}) (8)	r (mag) (9)	$F_{\rm AGN}$ (10)	$F_{\rm tidal}$ (11)
J00:02:49.07+00:45:04.8	0388	345	51793	0.0868	5.9	9.5	63	16.08	0	3
J00:02:49.44+00:45:06.7	0685	593	52203	0.0865	5.9	9.5	63	16.43	1	3
J00:02:57.21+00:07:50.5	0685	531	52203	0.0901	45.4	76.0	109	16.15	2	2
J00:02:58.59+00:08:31.0	0387	072	51791	0.0897	45.4	76.0	109	16.67	2	2
J00:03:23.74+01:05:47.3	1490	321	52994	0.0993	12.2	22.4	22	17.98	2	2
J00:03:23.74+01:05:59.5	0387	620	51791	0.0994	12.2	22.4	22	17.42	2	2
J00:04:25.78−09:58:54.4	0650	598	52143	0.1122	24.1	49.1	53	16.41	0	2
J00:04:26.66−09:58:34.4	0651	392	52141	0.1120	24.1	49.1	53	16.57	2	2
J00:04:31.92−01:14:11.7	0388	282	51793	0.0887	42.3	70.1	45	17.22	0	0
J00:04:33.25−01:13:34.4	1490	241	52994	0.0889	42.3	70.1	45	18.47	2	0

Notes. Column 1: SDSS names with J2000 coordinates given in the form of "hh:mm:ss.ss+dd:mm:ss.s"; Column 2: spectroscopic plate number; Column 3: Fiber ID; Column 4: modified Julian date; Column 6: angular separation; Column 7: transverse proper separation; Column 8: LOS velocity offset; Column 9: SDSS r-band model magnitude corrected for Galactic extinction; Column 10: flag for sub-populations in the parent AGN sample (refer to Section 2 for details). "0" through "2" are for narrow-line AGNs contained in the MPA-JHU DR7 catalog, where "0" stands for Seyferts, "1" for LINERs, and "2" for composites, respectively, according to the Kewley et al. (2001) and Kauffmann et al. (2003a) criteria for separating AGNs and composites from H II regions, and the Ho et al. (1997) criterion for separating Seyferts from LINERs (Figure 5). "3" for narrow-line quasars in the Reyes et al. (2008) sample but not in the MPA-JHU DR7 catalog, "4" for broad-line quasars, and "5" for broad-line AGNs according to the Hao et al. (2005b) selection; Column 11: flag from visual identification of tidal features (Section 2.3). "0" for "non-interaction," "1" for "ambiguous," "2" for "tidal," and "3" for "dumbbell" systems.

(This table is available in its entirety in a machine-readable form in the online journal. A portion is shown here for guidance regarding its form and content.)

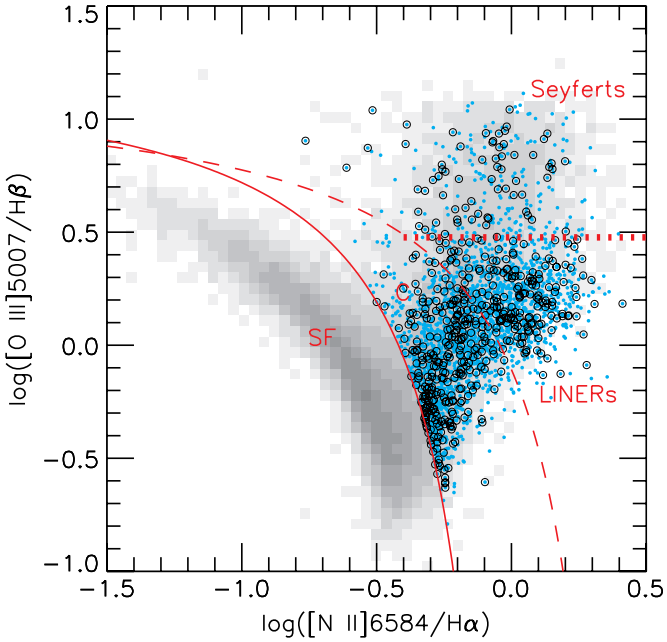

Figure 5. Diagnostic line ratios for AGNs in the pair sample (cyan dots) and those with tidal features (open circle). Gray scales indicate number densities of 31,179 emission-line galaxies from the SDSS DR4 (Kauffmann et al. 2003a). The solid curve displays the empirical separation between H II regions and AGNs (Kauffmann et al. 2003a), the dashed curve denotes the theoretical "starburst limit" from Kewley et al. (2001), and the dotted line represents the empirical division between Seyferts and LINERs (Ho et al. 1997). Pure star-forming ("SF") galaxies lie below the solid curve, AGN-dominated objects (Seyferts above and LINERs below the dotted line) lie above the dashed curve, and AGN-H II composites ("C") lie in between.

(A color version of this figure is available in the online journal.)

2002; Blanton et al. 2003). We correct for the fiber collision incompleteness by supplementing the observed AGN pairs with $(C-1)N_p$ systems randomly drawn from those with separation smaller than $55''$, where N_p is the observed number of pairs. Neglecting the tiny fraction of triples and higher multiples, the ratio between the intrinsic and the observed pair fraction is

$$C(f_{\rm lap}, p) = \frac{(1+2p)f_{\rm lap}f_{\rm spec,lap} + (1+p)(1-f_{\rm lap})f_{\rm spec}}{(1+2p)f_{\rm lap}f_{\rm spec,lap}^2}, \quad (3)$$

where $f_{\rm lap} \sim 30\%$ is the plate overlap fraction on the sky (Stoughton et al. 2002), p is the ratio of pairs to isolated galaxies, $f_{\rm spec,lap} \approx 0.99$ is the SDSS spectroscopic completeness in the plate overlap region, and $f_{\rm spec} \approx 0.92$ is the spectroscopic completeness in the un-overlapped region (Blanton et al. 2003). $C(f_{\rm lap}, p) \approx 1/f_{\rm lap} = 3.3$ when $p \ll 1$. We show in Figure 4 the distributions of redshift and projected separations of AGN pairs after correction for SDSS spectroscopic incompleteness. The corrected redshift distribution of the pair sample is similar to that of the parent AGNs, except that the pair sample is incomplete for projected angular separation $\lesssim 1\farcs4$ due to the imaging resolution limit of SDSS (the median point-spread function (PSF) FWHM of SDSS DR7 images is $1\farcs4$ in r; Abazajian et al. 2009). The corrected r_p distribution function increases with decreasing r_p (Figure 4).

2.3. AGN Pairs with Tidal Features

To mitigate contamination due to pairs that are closely separated but are not interacting and to focus on AGN pairs that are unambiguously experiencing strong tidal encounters, we further select from the AGN pair sample what we dub the "tidal" AGN pair sample by visually examining their SDSS images for optical tidal features such as bridges, tails, shells, or rings. We examine both the *gri*-color composite images (Lupton et al. 2004) and the calibrated FITS images in all five SDSS bands. We use visual identification as it should be more sensitive to low-surface-brightness (LSB) features and less subject to false positives than automated techniques like model fitting. While quantitative measures of mergers are more objective and yield reproducible results (e.g., Conselice 2003; Lotz et al. 2004), they may introduce biases toward certain merger stages (e.g., the first pericenter passage and the final coalescence; Lotz et al. 2008).

Table 2
Sample Summary

Selection (1)	Subsample (2)	Parent (3)	Pair (4)	Tidal (5)	Ambiguous (6)	Dumbbell (7)
$0.02 < z < 0.33$	NLAGN	129277	2529	501	327	20
	NLAGN-Kewley	50624	1583	312	190	18
	BLAGN	5564	79	9	10	0
	NLQSO	112	1	1	0	0
	QSO	3117	7	1	2	0
$0.02 < z < 0.16$, observed	NLAGN	112242	2488	482	322	20
	NLAGN-Kewley	44168	1555	299	186	18
	BLAGN	4595	78	8	10	0
	NLQSO	25	0	0	0	0
	QSO	279	2	0	1	0
$0.02 < z < 0.16$, corrected	NLAGN	112242	8116	2487	1377	118
	NLAGN-Kewley	44168	5035	1552	802	106
	BLAGN	4595	236	42	33	0
	NLQSO	25	0	0	0	0
	QSO	279	11	0	5	0

Notes. Column 1: selection criteria. The top block is the basic selection, the middle block is restricted to $z < 0.16$ to mitigate uncertainties due to small number statistics at higher redshifts, and the bottom block is after correction for incompleteness due to fiber collisions (Section 2.2.1); Column 2: subsamples in our selection of the parent AGN sample. "NLAGN": narrow-line AGNs according to the Kauffmann et al. (2003a) criterion which is our default, "NLAGN-Kewley": narrow-line AGNs according to the Kewley et al. (2001) criterion, "BLAGN": broad-line AGNs, "NLQSO": narrow-line quasars in the Reyes et al. (2008) sample but not in the MPA-JHU DR7 catalog, "QSO": broad-line quasars. Refer to Section 2 for details of each population; Column 3: number of AGNs in the parent AGN sample; Column 4: number of AGNs in the pair sample (Section 2.2); Columns 5–7: number of AGNs in the tidal, ambiguous, and dumbbell categories, respectively, according to our visual classification of the SDSS images. For details of each category, refer to Section 2.3.

We assign each pair a flag of "tidal," "ambiguous," "dumbbell" (discussed below), or "non-interaction" as listed in Table 1. We summarize the numbers of AGNs in each category in Table 2. To mitigate uncertainty of the visual inspection, one of us (X.L.) classified each object in the pair sample five times, with the order of objects scrambled each time and not knowing the results from previous identifications. The identification among five trials is identical for ∼80% of the objects; for objects with different classifications from each round (using "0" for non-interaction, "1" for ambiguous, and "2" for "tidal;" there are few "dumbbell" systems and their classification was almost always the same), we take the median as the final result. By inspecting the SDSS single-scan images we found 245 AGN pairs with unambiguous tidal features. In Figure 6, we show SDSS gri-color composite images of 36 such examples chosen to span the whole range of separations. The system shown in the third column and second row of Figure 6 is Mrk 266, which is a luminous infrared galaxy at $z = 0.028$. Its northern nucleus is optically classified as a Seyfert 2, whereas the southern nucleus is a LINER. Its double AGN nature is confirmed by *Chandra* X-ray observations (Mazzarella et al. 2011; see also Brassington et al. 2007 and Wang & Gao 2010).

2.3.1. "Ambiguous" and "Dumbbell" Systems

We excluded from our tidal sample those objects we call "ambiguous" pairs of AGNs in which both members exhibit ordered bar or spiral features but show no clear signs of galaxy–galaxy interactions. While these bar or spiral features could arise from galaxy–galaxy interactions, they may also be induced by internal instabilities. There are 169 "ambiguous" pairs and we show six examples in Figure 7. We rejected these pairs because they are not as convincing as pairs with clear merger-induced tidal features (such as disruptive asymmetries or tidal bridges).

In addition, we excluded ten "dumbbell" systems (e.g., Valentijn & Casertano 1988), which have double nuclei in a single host galaxy, but show no optical tidal features indicative of ongoing interactions between the two nuclei. Figure 8 shows six such examples. Three of the ten systems contain disk components, whereas the others have optical morphologies reminiscent of 3C75. 3C75 is a double radio source at the center of the galaxy cluster A400 which shows evidence for interactions only in its twin radio jets (Owen et al. 1985; Lauer 1988; Beers et al. 1992). We did not find evidence for interactions in the radio by examining the FIRST (Becker et al. 1995; White et al. 1997) images of the "dumbbell" pairs, although neither the spatial resolution nor sensitivity is high enough for a strong constraint.

2.3.2. Using the Co-added SDSS Stripe 82 Images to Identify Low-surface-brightness Features

Our identification for tidal features is limited by the surface brightness sensitivity and resolving power of the SDSS images. The limiting magnitude of individual SDSS scan images with a S/N of 5 is $r = 23.1$ mag (in the AB system) for stars (Gunn et al. 1998). To quantify the number of interacting AGNs with LSB tidal features below the sensitivity of individual SDSS scan images (e.g., Smirnova et al. 2010), we examine the co-added images of a subset of AGNs that are located in the SDSS Stripe 82.[9] Stripe 82 is a sky region covering ∼270 deg^2 along the Celestial Equator in the Southern Galactic Cap, which the SDSS has imaged ∼100 times, producing co-added images ∼2 mag more sensitive than individual scan images (Abazajian et al. 2009).

We find that ∼ 27% of AGN pairs (6 of 22 pairs) in the "ambiguous" category show tidal features in the co-added

[9] www.sdss.org/legacy/stripe82.html

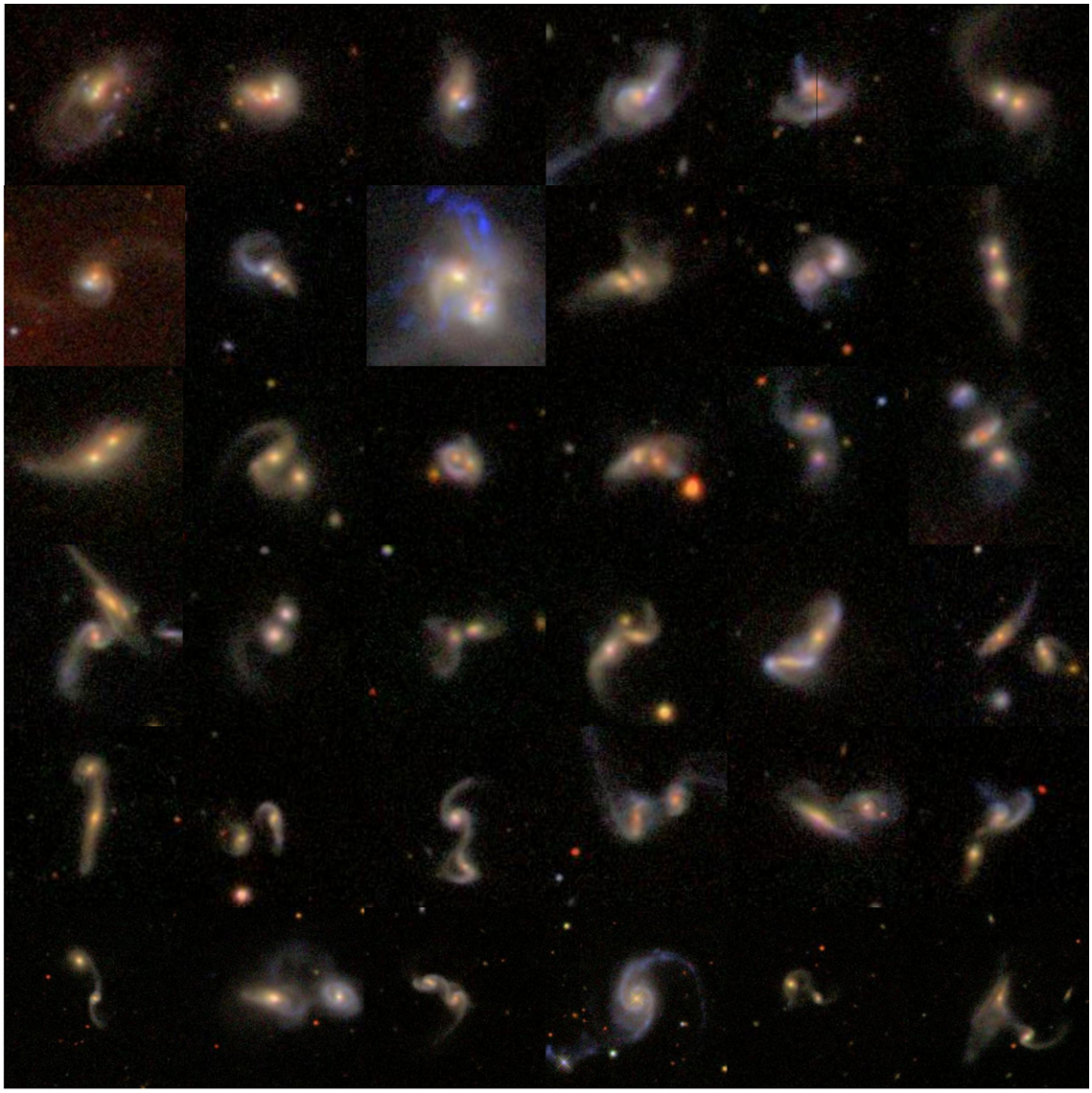

Figure 6. SDSS gri-color composite images of 36 examples of AGN pairs with tidal features. North is up and east is to the left. The FOV of each panel is $50'' \times 50''$, except for those in the last row whose FOV is $100'' \times 100''$. Objects are arranged in increasing order of transverse proper separation r_p from left to right and from top to bottom. Binary AGNs in the first, second, third, fourth, fifth, and last row have $r_p < 5$, $5 < r_p < 10$, $10 < r_p < 15$, $15 < r_p < 20$, $20 < r_p < 30$, and $30 < r_p < 100\,h_{70}^{-1}$ kpc, respectively. The median redshift of the sample is 0.08.

(A color version of this figure is available in the online journal.)

Stripe 82 images; the lower sideband (LSB) missing fraction is lower ($\sim$ 8.5%, 5 of 58 pairs) for the "non-interaction" category. Figure 9 shows two such examples. We correct for the LSB missing fraction using these estimates of the fraction of the "ambiguous" and "non-interaction" cases in what follows. The LSB correction factor depends on redshift, since the LSB feature detection is redshift dependent due to the limited image resolution. Here what we have estimated using the co-added images is the effective LSB correction factor averaged over the redshift range spanned by the sample, which should be a reasonable approximation as the redshift distribution of the Stripe 82 subsample is similar to the parent pair sample. We supplement the tidal AGN pair sample with the 11 pairs identified using the co-added Stripe 82 images. Our final AGN pair sample with tidal features consists of 256 AGN pairs. Table 2 lists the numbers of AGNs in each category. The fraction of AGN–H II composites with tidal features (out of all composites in AGN pairs) is consistent with that of the other AGNs (i.e., narrow-line AGNs that satisfy the Kewley et al. 2001 criterion plus those in the other AGN categories as discussed in Section 2) with tidal features (out of all the other AGNs in pairs). Among the 512 AGNs in the tidal sample, 501 AGNs are contained in the MPA-JHU SDSS DR7 galaxy catalog, whose diagnostic line ratios are shown in Figure 5; the other 11 objects are selected as either narrow-line or broad-line quasars. In the Appendix, we show the SDSS images and fiber spectra for three examples of AGN pairs with tidal features.

2.4. Selection Incompleteness

The primary factors that limit the sample completeness include the resolution and surface-brightness limits of SDSS photometry, fiber collisions, the limitations of visual identification of tidal features, and the heterogeneity of the parent sample.

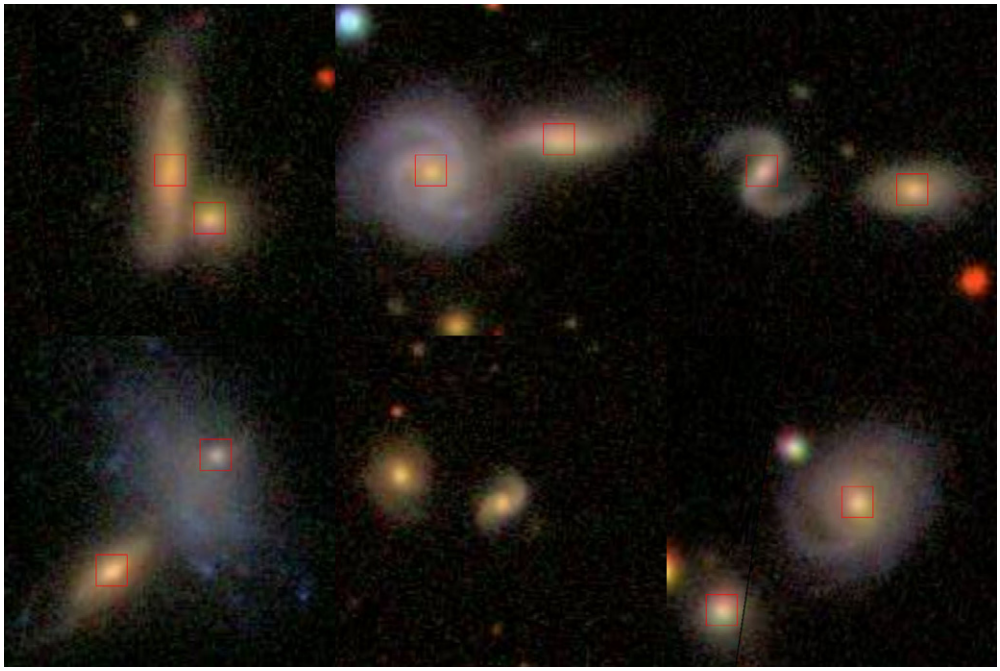

Figure 7. Examples of ambiguous systems in the pair sample. Objects are arranged in increasing order of transverse proper separation r_p from left to right and from top to bottom. The FOV of each image tile is $50'' \times 50''$. We mark the targets with red boxes when additional objects are within the FOV shown.
(A color version of this figure is available in the online journal.)

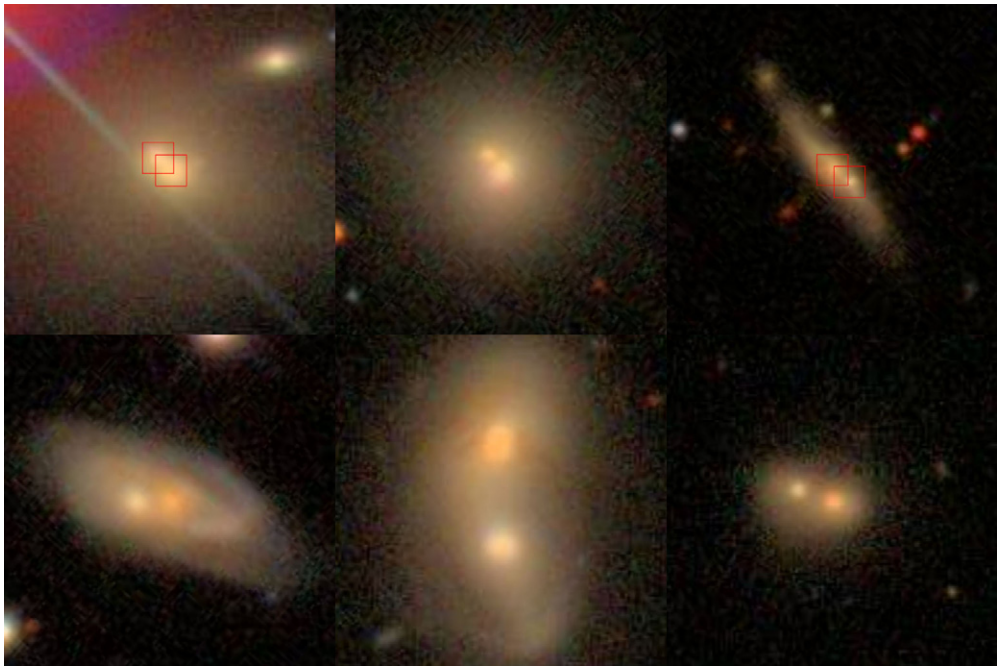

Figure 8. Same as Figure 7, but for example dumbbell systems in the pair sample. For the systems shown, r_p ranges from 2.3 to $9.5\,h_{70}^{-1}$ kpc. The long spike in the upper left panel is due to diffraction from a nearby star.
(A color version of this figure is available in the online journal.)

Our approach is insensitive to AGN pairs in advanced mergers with nuclear separations that are too small to be resolved by the deblending algorithm of SDSS photometry (Lupton et al. 2001). Pairs with nuclear separations $\lesssim 1\farcs4$ will not be included. At $z = 0.16$, $1''$ corresponds to 2.7 kpc in the assumed cosmology and therefore the sample is incomplete for $r_p \lesssim 5\,h_{70}^{-1}$ kpc. At the low-redshift end, the separation limit is set intrinsically by galaxy size, which is a function of stellar mass. AGNs in the pair sample have a median stellar mass $\log(M_*/M_\odot) = 10.8$ using the stellar mass estimates of Kauffmann et al. (2003b). The z-band half light radius is observed to be $\sim$3.3 kpc for this stellar mass (Kauffmann et al. 2003c).

Our tidal sample does not include mergers at very early stages before the first pericenter passage; such objects have no detectable tidal features (Toomre & Toomre 1972). In addition, the strength of the tidally induced features does

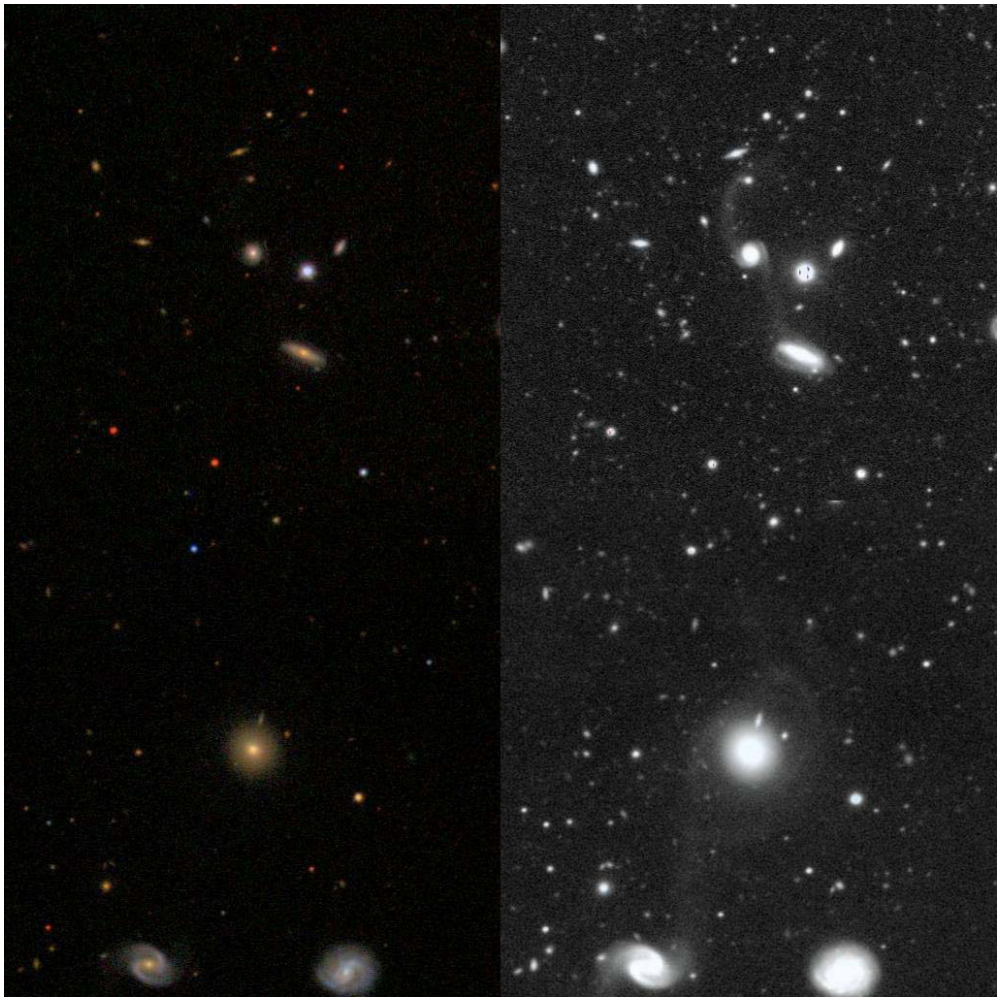

Figure 9. Identifying low surface-brightness tidal features using the co-added Stripe 82 images. We show two examples of interacting AGN pairs which show tidal features in the co-added Stripe 82 images but not in individual SDSS scan images. North is up and east is to the left. The left columns are SDSS *gri*-color composite images from individual scans, whereas the right columns show the co-added *r*-band images in Stripe 82. The FOV of each panel is $200'' \times 200''$. The FOV is centered on one of the AGNs in the pair, which is connected to the other galaxy via a tidal stream visible in the co-added images.

(A color version of this figure is available in the online journal.)

not increase monotonically with decreasing separation when the merger advances to later stages; it also depends on the progenitor host-galaxy properties and orbital parameters. We keep these separation-dependent limitations and biases in mind when discussing our results, although we do not attempt to correct for them. Additional populations of mergers without discernable optical tidal features may include minor mergers whose mass ratios are larger than ∼30 (Lotz et al. 2010), spheroidal mergers with large bulge-to-disk ratios (Mihos & Hernquist 1996), and mergers on significantly retrograde orbits (Toomre & Toomre 1972). Some of these biases are mass or morphology-dependent and therefore can be corrected for using control samples matched in galaxy stellar mass (Paper II).

3. RESULT: THE FREQUENCY OF AGN PAIRS WITH $5\,h_{70}^{-1}$ kpc $\lesssim r_p < 100\,h_{70}^{-1}$ kpc AT $z \sim 0.1$

The fraction of AGN pairs with $5\,h_{70}^{-1}$ kpc $\lesssim r_p < 100\,h_{70}^{-1}$ kpc among the parent AGN sample at $0.02 < z < 0.16$ is $f_{\rm p,obs} \approx 1.1\%$ (1265 systems out of 117,141 AGNs) before correction for SDSS spectroscopic incompleteness and is $f_{\rm p} \approx 3.6\%$ after correction. As the pair sample may contain false positives due to closely separated pairs that are not (yet) interacting, this serves as an upper limit for the intrinsic fraction of interacting AGN pairs.

Figure 10 shows redshift versus transverse proper separation and the distributions of these two quantities for AGN pairs with tidal features. There are only nine pairs at $z > 0.16$. This apparent deficiency likely results mainly from the combination of fewer objects in the parent sample and the decreasing apparent size of tidal features with redshift. The redshift distribution of the tidal sample is roughly consistent with the parent sample both before and after correction for fiber collisions, except that the tidal sample is incomplete for smaller separation pairs (projected angular separation $\lesssim 2''$). The number of tidal pairs found increases with decreasing r_p (except for the bin at the smallest scales, which is affected by the resolution limit of SDSS photometry), a trend that is partly caused by the fact that closer pairs tend to show more prominent tidal features.

We estimate the fraction of AGN pairs with tidal features among the parent AGNs at $0.02 < z < 0.16$ as

$$f_{\rm t} = C(f_{\rm lap}, p) f_{\rm t,obs} = C(f_{\rm lap}, p) \frac{(N_t + C_a N_a + C_n N_n)}{2N}, \quad (4)$$

where $C(f_{\rm lap}, p) \approx 3.3$ is the correction factor for spectroscopic incompleteness (Equation (3)), N_t is the number of galaxies in

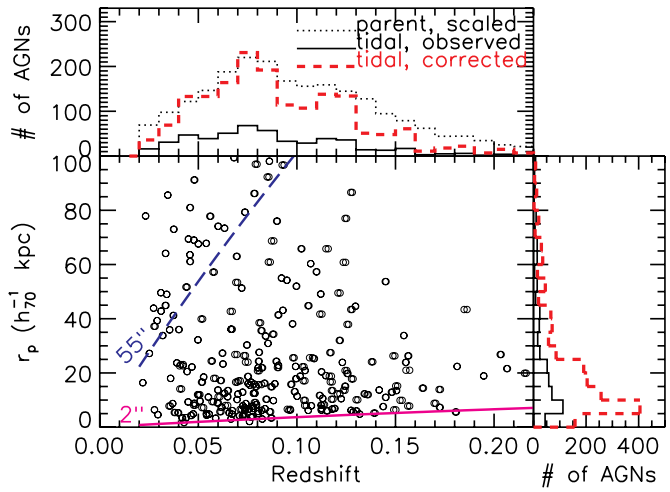

Figure 10. Redshift vs. projected separation (r_p) for AGN pairs with tidal features. The meanings of the lines are the same as in Figure 4.

(A color version of this figure is available in the online journal.)

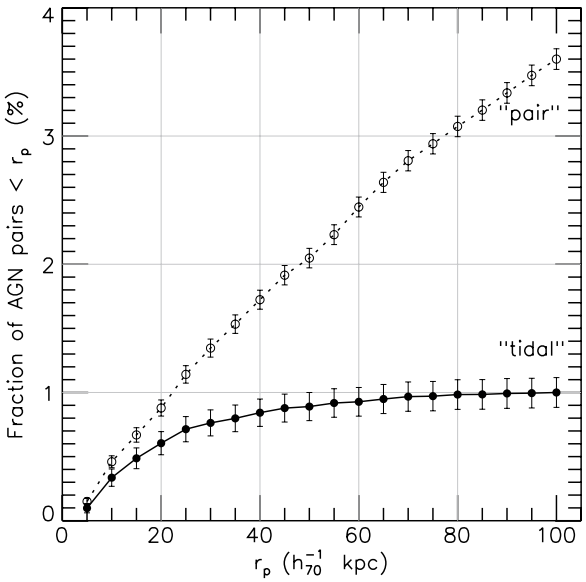

Figure 11. Cumulative fraction of AGN pairs with projected separations smaller than r_p. Open circles denote AGN pairs, whereas filled circles represent the subset with tidal features. The quoted uncertainties are Poisson errors.

AGN pairs with tidal features identified in individual SDSS images, N_a and N_n are the numbers of galaxies classified as "ambiguous" and "non-interaction," $C_a = 27\%$ and $C_n = 8.5\%$ are the correction factors for LSB features estimated based on our Stripe 82 experiment (Section 2.3.2), and N is the number of AGNs in the parent sample. We find $f_{\rm t,obs} \approx 0.3\%$ before correction for spectroscopic incompleteness and $f_{\rm t} \approx 1.0\%$ after correction. Because the tidal sample is incomplete for interacting AGN pairs without detectable tidal features, this serves as a lower limit for the intrinsic fraction of interacting AGN pairs.

Figure 11 presents how our results vary as a function of upper limit of r_p. Observations of statistical samples of inactive galaxy pairs suggest that $\sim 30\,h_{70}^{-1}$ kpc is the physical scale in projected separation below which galaxy pairs exhibit significantly higher star formation rates than field galaxies (e.g., Barton et al. 2000; Lambas et al. 2003; Alonso et al. 2004; Nikolic et al. 2004). The fraction of AGN pairs with $5\,h_{70}^{-1}$ kpc $\lesssim r_p < 30\,h_{70}^{-1}$ kpc is 1.3%, among which ~60% show tidal features.

The fraction of AGN pairs we measure depends on the sensitivity of our AGN identification. We adopted an S/N of 3 as our baseline value for the detection threshold of the diagnostic emission lines, Hβ, [O III] λ5007, Hα, and [N II] λ6584, in the selection of narrow-line AGNs. We now address how the S/N threshold affects our results for the fraction of AGN pairs. The sample statistics are dominated by narrow-line AGNs (Table 2), and we thus neglect the effects of changing the selection criteria for the other AGN categories. In the left panel of Figure 12, we show the S/N distribution of the four diagnostic emission lines, for AGNs in the parent, pair, and tidal samples (both corrected for fiber incompleteness for the latter two), respectively. For these four emission lines, AGNs in the pair sample have similar S/N distributions to those of the parent AGN sample. On the other hand, AGNs in the tidal sample have larger emission-line S/N than do the parent AGNs; tidal AGNs have median emission-line S/N which are ~1.5 times those of parent AGNs. This may be explained if AGN pairs with more prominent tidal features tend to exhibit stronger emission lines (and thereby have higher S/N detections). We increase the S/N threshold and redo the analysis. In the right panel of Figure 12, we show how the fraction of AGN pairs (and those with tidal features) varies with increasing S/N threshold. The fraction of AGN pairs drops from ~3.6% at S/N > 3 to ~1.4% at S/N $\gtrsim$ 30. Because the pair and parent samples have similar S/N distributions, the pair fraction would scale $\propto N^2/N \propto N$ if AGNs were uncorrelated (i.e., randomly paired), where N denotes the total number of parent AGNs. The observed decay of pair fraction with decreasing N is less steep than the uncorrelated case would predict. The fraction of AGN pairs with detected tidal features roughly stays constant with increasing S/N threshold, although we caution that it should be treated as a lower limit and the incompleteness due to the inspection of tidal features is likely higher at lower S/N, if AGN pairs with more prominent tidal features tend to exhibit stronger emission lines. At S/N $\gtrsim$ 15, $\gtrsim$80% of all AGN pairs show tidal features (Figure 12).

4. DISCUSSION

4.1. Implications for AGN Pairs with Smaller Separations

The fraction of AGN pairs at $0.02 < z < 0.16$ with $5\,h_{70}^{-1}$ kpc $\lesssim r_p < 100\,h_{70}^{-1}$ kpc is ~3.6% corrected for SDSS spectroscopic incompleteness. The pair fraction decreases to ~1.0% if we restrict ourselves to those pairs that show clear tidal features in SDSS images. If we assume that (1) the fraction of observed pairs within a certain range of projected separations scales linearly with the time τ that a merger spends in that range, and (2) the probability that the two AGNs in a merger are simultaneously active does not strongly depend on the merging phase over the range of separations we are considering (i.e., a few kpc to tens-of-kpc scales), then the fraction of AGN pairs on tens-of-kpc scales can be related to the fraction on kpc scales as $f_{\rm kpc} \approx f_{\rm tens\text{-}of\text{-}kpc}\tau_{\rm kpc}/\tau_{\rm tens\text{-}of\text{-}kpc}$. The timescales τ are proportional to the length scales, so $f_{\rm kpc}$ will be ~0.1% or ~0.4% using the tidal and full pair samples, respectively.

Several studies (Liu et al. 2010b; Smith et al. 2010; Wang et al. 2009) have found that ~1% of SDSS AGNs show double-peaked profiles in [O III] $\lambda\lambda$4959,5007 emission lines, in which the two velocity peaks are blueshifted and redshifted from the systemic velocity determined from stellar absorption lines. As shown in Shen et al. (2010b), at least ~50% of the double-peaked narrow emission lines are due to narrow-line region kinematics such

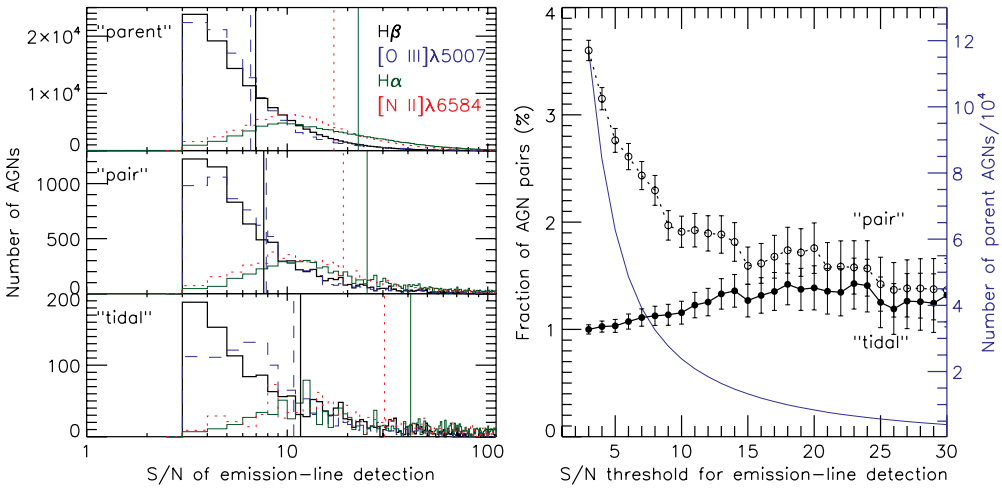

Figure 12. Left: S/N distributions of diagnostic emission-line detection of AGNs in the parent, pair, and tidal samples (after correction for spectroscopic incompleteness). Vertical lines indicate the median values for each distribution. Right: dependence of the fraction of AGN pairs on the S/N threshold adopted for emission-line detection (for all four emission lines for both AGNs in a pair). Open circles denote AGN pairs, whereas filled circles represent the subset with tidal features. The quoted uncertainties are Poisson errors. The blue solid curve displays the total number of AGNs in the parent sample as a function of S/N threshold.

(A color version of this figure is available in the online journal.)

as biconical outflows or rotating disks (e.g., Axon et al. 1998; Veilleux et al. 2001; Crenshaw et al. 2010), while ∼10% or more reflect the orbital motion of a merging pair of AGNs (e.g., Zhou et al. 2004; Comerford et al. 2009a). In the merging AGN pair scenario for those double-peaked AGNs, the projected angular separation of the two nuclei has to be smaller than 3″ for both AGNs to be covered by a single SDSS fiber. This corresponds to $r_p < 8\,h_{70}^{-1}$ kpc for the typical redshift of $z \sim 0.15$ in the Liu et al. (2010b) sample. The fraction of AGNs in kpc-scale pairs we have inferred ($f_{\rm kpc} \sim 0.1\%$–0.4%) suggests that only ∼ 10%–40% of AGNs with double-peaked narrow emission lines are merging systems. However, this should be treated as an upper limit, considering there are kpc-scale AGN pairs with LOS velocity offsets <150 km s^{-1} and therefore will not be identified as SDSS double-peaked narrow-line AGNs. We caution that the estimate is highly uncertain since $\tau_{\rm kpc}/\tau_{\rm tens\text{-}of\text{-}kpc}$ depends on merger parameters and the host-galaxy properties of AGN pairs. In addition, we use the Kauffmann et al. (2003a) criterion for diagnostic line ratios, whereas the Kewley et al. (2001) criterion was adopted in the Liu et al. (2010b) sample, whose S/N cut for spectral measurements was also more stringent. Nevertheless, Liu et al. (2010a) used follow-up observations to confirm four kpc-scale binary AGNs out of 43 double-peaked objects of the Liu et al. (2010b) sample (see also Shen et al. 2010b), in broad agreement with our estimate of $f_{\rm kpc}$ based on AGN pairs with broader separations.

4.2. Comparison with Binary Quasars

The fraction of quasars in pairs (with bolometric luminosities of $\gtrsim 10^{46}$ erg s^{-1}) with separations of tens to hundreds of kpc is $\lesssim$0.1% at $1 < z < 5$ (e.g., Hennawi et al. 2006, 2010; Myers et al. 2008; Shen et al. 2010a). This is ∼8–30 times smaller than what we observe for the less luminous AGN pairs at $\bar{z} \sim 0.08$. If we assume that (1) all luminous high-redshift quasars are triggered in galaxy–galaxy mergers, and (2) the two quasars in a pair shine at random, uncorrelated times, among all quasars the observed fraction of quasar pairs with separations of tens to hundreds of kpc will be roughly the ratio of the quasar lifetime $\tau_{\rm quasar}$ and the time for two galaxies with this separation to merge $\tau_{\rm merge}$. Both $\tau_{\rm quasar}$ and $\tau_{\rm merge}$ span orders of magnitude in their parameter spaces. We speculate that the first of the two assumptions is likely valid for high-redshift luminous quasars, as mergers are arguably the most efficient mechanism to give rise to such high-mass accretion rates. The second assumption is valid, provided that the separations of observed quasar pairs (only a few of which are tens-of-kpc separations) are too large for galaxy–galaxy tidal interactions to be effective (the counterexample of an interacting quasar pair reported by Green et al. 2010 has a separation of 21 kpc which is at the lower bound of known quasar pairs). However, these two assumptions do not necessarily apply to the less luminous AGN pairs; their intrinsic accretion luminosities are roughly three orders of magnitude lower, and the typical projected separations in our sample are smaller by a factor of ∼10 than the high-redshift luminous quasar pairs. Our AGN pair sample (low-luminosity, low-redshift) and the (luminous, high-redshift) binary quasar samples probe populations at very different redshift and AGN-luminosity regimes, such that a useful direct comparison with the binary quasar samples cannot be made within our sample. In particular, the statistics of our sample is dominated by Seyfert galaxies (and mostly narrow-line Seyferts; Table 2).

4.3. What Fraction of Moderate-luminosity AGNs Are Triggered in Galaxy Interactions?

As above, if we assume that all moderate-luminosity AGNs were triggered in galaxy interactions and the two components in a pair shone at uncorrelated times, the fraction of AGNs in pairs with $5\,h_{70}^{-1}$ kpc $< r_p < 100\,h_{70}^{-1}$ kpc would roughly be the ratio between the typical lifetime of moderate-luminosity AGNs $\tau_{\rm AGN}$ and the dynamical timescale of galaxy mergers with $5\,h_{70}^{-1}$ kpc $< r_p < 100\,h_{70}^{-1}$ kpc $\tau_{5-100\,\rm kpc}$, which is ∼10% assuming $\tau_{\rm AGN} \sim 10^8$ yr and $\tau_{5-100\,\rm kpc} \sim 10^9$ yr, larger than the ∼1%–4% value that we have found. This implies that only $\sim 10\%\text{–}40\% \times (10^8\ {\rm yr}/\tau_{\rm AGN})(\tau_{5-100\,\rm kpc}/10^9\ {\rm yr})$ of moderate-luminosity AGNs can be triggered in galaxy interactions. In addition, we will show in Paper II that the strengths of AGN activity are correlated between the two components in interacting pairs. This correlation suggests that the two SMBHs in a galaxy pair may tend to be activated simultaneously, making the expected fraction of AGN pairs even larger than $\sim\tau_{\rm AGN}/\tau_{5-100\,\rm kpc}$.

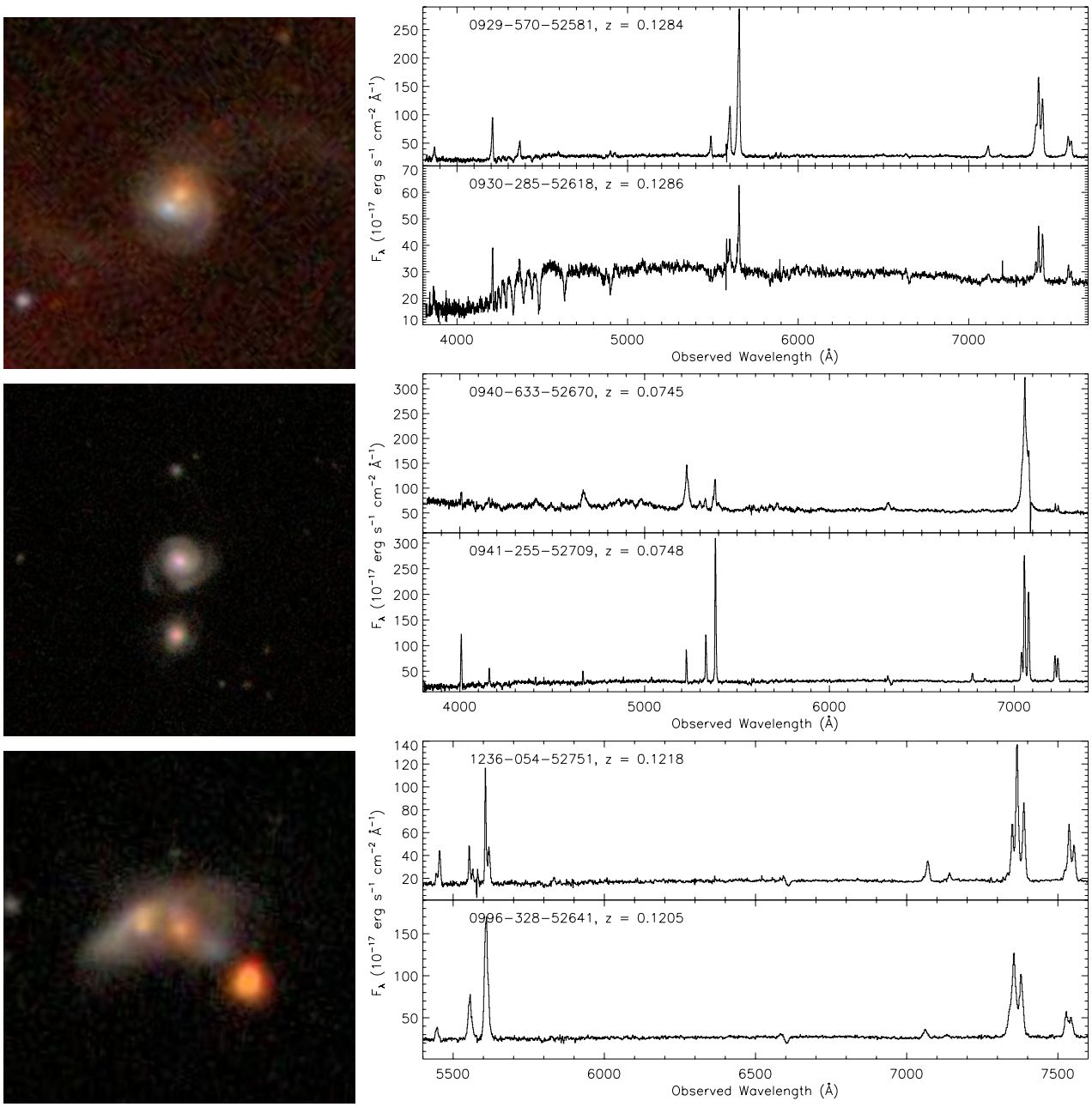

Figure 13. Three examples of AGN pairs with tidal features. Left column: SDSS *gri*-color composite images. North is up and east is to the left. FOV is $50'' \times 50''$ for the top and bottom objects, and $100'' \times 100''$ for the middle one. Right column: SDSS fiber spectra. Labeled on each panel are spectroscopic plate number, fiber ID, and modified Julian date. Top: 0929-570-52581 is the NW component, and 0930-285-52618 is the SE component. The two AGNs are separated by $2''.4$ ($5.6\,h_{70}^{-1}$ kpc). Middle: the northern component (940-633-52670) is a broad-line, and the southern component (941-255-52709) is a narrow-line AGN. They are separated by $21''.3$ ($30.3\,h_{70}^{-1}$ kpc). Bottom: 1236-54-52751 is the western component which has double-peaked narrow-emission lines, and 996-328-52641 is the eastern component. The two AGNs are separated by $5''.7$ ($12.3\,h_{70}^{-1}$ kpc). The object to the SW is a foreground star.
(A color version of this figure is available in the online journal.)

Thus, the observed fraction of AGN pairs suggests that fewer than $\sim$10%–40% $\times$ (10^8 yr/$\tau_{\rm AGN}$)($\tau_{5-100\ {\rm kpc}}/10^9$ yr) of moderate-luminosity AGNs are triggered in galaxy interactions.

5. SUMMARY

We have selected a sample of 1286 AGN pairs (or multiples) with LOS velocity offsets $<$600 km s^{-1} and projected separations $<100\,h_{70}^{-1}$ kpc from 138,070 optical AGNs in SDSS DR7. Two hundred and fifty-six pairs of these show unambiguous morphological tidal features in their SDSS images indicative of ongoing interactions. After correction for spectroscopic incompleteness, the fraction of AGN pairs with $5\,h_{70}^{-1}$ kpc $\lesssim r_p \leqslant 100\,h_{70}^{-1}$ kpc and $\Delta v < 600$ km s^{-1} is $\sim$3.6% among the parent AGNs at $0.02 < z < 0.16$. The fraction of AGN pairs that show tidal features is $\sim$1.0%.

The current study is a part of our continuing effort to systematically identify and characterize the populations of merging SMBHs at various stages. The sample that we have presented increases the number of known AGN pairs on $\sim$5–$100\,h_{70}^{-1}$ kpc scales by more than an order of magnitude, thanks to the statistical power of SDSS. It constitutes the starting point of a statistical analysis of their properties. In Paper II, we will

examine the effects of tidal interactions on AGN pairs by quantifying their recent star formation and BH accretion activity as a function of pair separation, calibrated against a control sample of AGNs matched in both redshift and stellar mass distribution, and we will examine correlations between the interacting components.

We thank J. Greene and P. Kampczyk for helpful comments, and an anonymous referee for a prompt and careful report. We are grateful to the MPA-JHU team, especially J. Brinchmann, who have made their catalog of derived galaxy properties publicly available. X.L. and M.A.S. acknowledge the support of NSF grant AST-0707266. Support for the work of X.L. was provided by NASA through an Einstein Postdoctoral Fellowship grant number PF0-110076 awarded by the Chandra X-ray Center, which is operated by the Smithsonian Astrophysical Observatory for NASA under contract NAS8-03060. Y.S. acknowledges support from a Clay Postdoctoral Fellowship through the Smithsonian Astrophysical Observatory.

Funding for the SDSS and SDSS-II has been provided by the Alfred P. Sloan Foundation, the Participating Institutions, the National Science Foundation, the U.S. Department of Energy, the National Aeronautics and Space Administration, the Japanese Monbukagakusho, the Max Planck Society, and the Higher Education Funding Council for England. The SDSS website is www.sdss.org/.

The SDSS is managed by the Astrophysical Research Consortium for the Participating Institutions. The Participating Institutions are the American Museum of Natural History, Astrophysical Institute Potsdam, University of Basel, University of Cambridge, Case Western Reserve University, University of Chicago, Drexel University, Fermilab, the Institute for Advanced Study, the Japan Participation Group, Johns Hopkins University, the Joint Institute for Nuclear Astrophysics, the Kavli Institute for Particle Astrophysics and Cosmology, the Korean Scientist Group, the Chinese Academy of Sciences (LAMOST), Los Alamos National Laboratory, the Max-Planck-Institute for Astronomy (MPIA), the Max-Planck-Institute for Astrophysics (MPA), New Mexico State University, Ohio State University, University of Pittsburgh, University of Portsmouth, Princeton University, the United States Naval Observatory, and the University of Washington.

Facility: Sloan

APPENDIX

EXAMPLES OF AGN PAIRS WITH TIDAL FEATURES

In Figure 13, we show SDSS images and spectra for three examples of AGN pairs with tidal features. Note that for AGN pairs with small (kpc-scale) separations (e.g., the top object shown in Figure 13), we cannot rule out the possibility that one AGN is ionizing both galaxies (e.g., Liu et al. 2010a). High-resolution X-ray and/or radio observations can help better constrain the double or single AGN nature of these sources.

REFERENCES

Abazajian, K. N., Adelman-McCarthy, J. K., Agäueros, M. A., et al. 2009, ApJS, 182, 543
Adelman-McCarthy, J. K., Agüeros, M. A., Allam, S. S., et al. 2008, ApJS, 175, 297
Aihara, H., Allende Prieto, C., An, D., et al. 2011, ApJS, 193, 29
Alonso, M. S., Tissera, P. B., Coldwell, G., & Lambas, D. G. 2004, MNRAS, 352, 1081
Armitage, P. J., & Natarajan, P. 2002, ApJ, 567, L9
Axon, D. J., Marconi, A., Capetti, A., et al. 1998, ApJ, 496, L75
Baldwin, J. A., Phillips, M. M., & Terlevich, R. 1981, PASP, 93, 5
Ballo, L., Braito, V., Della Ceca, R., et al. 2004, ApJ, 600, 634
Barth, A. J., Bentz, M. C., Greene, J. E., & Ho, L. C. 2008, ApJ, 683, L119
Barton, E. J., Geller, M. J., & Kenyon, S. J. 2000, ApJ, 530, 660
Becker, R. H., White, R. L., & Helfand, D. J. 1995, ApJ, 450, 559
Beers, T. C., Gebhardt, K., Huchra, J. P., et al. 1992, ApJ, 400, 410
Begelman, M. C., Blandford, R. D., & Rees, M. J. 1980, Nature, 287, 307
Bianchi, S., Chiaberge, M., Piconcelli, E., Guainazzi, M., & Matt, G. 2008, MNRAS, 386, 105
Blanton, M. R., Lin, H., Lupton, R. H., et al. 2003, AJ, 125, 2276
Blanton, M. R., Schlegel, D. J., Strauss, M. A., et al. 2005, AJ, 129, 2562
Brassington, N. J., Ponman, T. J., & Read, A. M. 2007, MNRAS, 377, 1439
Brinchmann, J., Charlot, S., White, S. D. M., et al. 2004, MNRAS, 351, 1151
Bruzual, G., & Charlot, S. 2003, MNRAS, 344, 1000
Colpi, M., & Dotti, M. 2009, arXiv:0906.4339
Comerford, J. M., Gerke, B. F., Newman, J. A., et al. 2009a, ApJ, 698, 956
Comerford, J. M., Griffith, R. L., Gerke, B. F., et al. 2009b, ApJ, 702, L82
Conselice, C. J. 2003, ApJS, 147, 1
Crenshaw, D. M., Schmitt, H. R., Kraemer, S. B., Mushotzky, R. F., & Dunn, J. P. 2010, ApJ, 708, 419
Darg, D. W., Kaviraj, S., Lintott, C. J., et al. 2010, MNRAS, 401, 1043
Dotti, M., Colpi, M., Haardt, F., & Mayer, L. 2007, MNRAS, 379, 956
Eisenstein, D. J., Annis, J., Gunn, J. E., et al. 2001, AJ, 122, 2267
Ellison, S. L., Patton, D. R., Simard, L., & McConnachie, A. W. 2008, AJ, 135, 1877
Goulding, A. D., & Alexander, D. M. 2009, MNRAS, 398, 1165
Green, P. J., Myers, A. D., Barkhouse, W. A., et al. 2010, ApJ, 710, 1578
Gunn, J. E., Carr, M., Rockosi, C., et al. 1998, AJ, 116, 3040
Haehnelt, M. G. 1994, MNRAS, 269, 199
Hao, L., Strauss, M. A., Fan, X., et al. 2005a, AJ, 129, 1795
Hao, L., Strauss, M. A., Tremonti, C. A., et al. 2005b, AJ, 129, 1783
Hennawi, J. F., Myers, A. D., Shen, Y., et al. 2010, ApJ, 719, 1672
Hennawi, J. F., Strauss, M. A., Oguri, M., et al. 2006, AJ, 131, 1
Ho, L. C., Filippenko, A. V., & Sargent, W. L. W. 1997, ApJS, 112, 315
Holz, D. E., & Hughes, S. A. 2005, ApJ, 629, 15
Kauffmann, G., Heckman, T. M., Tremonti, C., et al. 2003a, MNRAS, 346, 1055
Kauffmann, G., Heckman, T. M., White, S. D. M., et al. 2003b, MNRAS, 341, 33
Kauffmann, G., Heckman, T. M., White, S. D. M., et al. 2003c, MNRAS, 341, 54
Kewley, L. J., Dopita, M. A., Sutherland, R. S., Heisler, C. A., & Trevena, J. 2001, ApJ, 556, 121
Komossa, S., Burwitz, V., Hasinger, G., et al. 2003, ApJ, 582, L15
Kormendy, J., & Richstone, D. 1995, ARA&A, 33, 581
Koss, M., Mushotzky, R., Veilleux, S., & Winter, L. 2010, ApJ, 716, L125
Lambas, D. G., Tissera, P. B., Alonso, M. S., & Coldwell, G. 2003, MNRAS, 346, 1189
Lauer, T. R. 1988, ApJ, 325, 49
Liu, X., Greene, J. E., Shen, Y., & Strauss, M. A. 2010a, ApJ, 715, L30
Liu, X., Shen, Y., & Strauss, M. A. 2011a, arXiv:1104.0951
Liu, X., Shen, Y., & Strauss, M. A. 2011b, ApJ, 736, L7
Liu, X., Shen, Y., Strauss, M. A., & Greene, J. E. 2010b, ApJ, 708, 427
Liu, X., Zakamska, N. L., Greene, J. E., et al. 2009, ApJ, 702, 1098
Lotz, J. M., Jonsson, P., Cox, T. J., & Primack, J. R. 2008, MNRAS, 391, 1137
Lotz, J. M., Jonsson, P., Cox, T. J., & Primack, J. R. 2010, MNRAS, 404, 575
Lotz, J. M., Primack, J., & Madau, P. 2004, AJ, 128, 163
Lupton, R., Blanton, M. R., Fekete, G., et al. 2004, PASP, 116, 133
Lupton, R., Gunn, J. E., Ivezić, Z., Knapp, G. R., & Kent, S. 2001, in ASP Conf. Ser. 238, Astronomical Data Analysis Software and Systems X, ed. F. R. Harnden, Jr., F. A. Primini, & H. E. Payne (San Francisco, CA: ASP), 269
Mazzarella, J. M., Iwasawa, K., Vavilkin, T., et al. 2011, AJ, submitted
Mihos, J. C., & Hernquist, L. 1996, ApJ, 464, 641
Milosavljević, M., & Merritt, D. 2001, ApJ, 563, 34
Myers, A. D., Richards, G. T., Brunner, R. J., et al. 2008, ApJ, 678, 635
Nikolic, B., Cullen, H., & Alexander, P. 2004, MNRAS, 355, 874
O'Donnell, J. E. 1994, ApJ, 422, 158
Osterbrock, D. E., & Pogge, R. W. 1985, ApJ, 297, 166
Owen, F. N., O'Dea, C. P., Inoue, M., & Eilek, J. A. 1985, ApJ, 294, L85
Piconcelli, E., Vignali, C., Bianchi, S., et al. 2010, ApJ, 722, L147
Reyes, R., Zakamska, N. L., Strauss, M. A., et al. 2008, AJ, 136, 2373
Richards, G. T., Fan, X., Newberg, H. J., et al. 2002, AJ, 123, 2945
Richstone, D., Ajhar, E. A., Bender, R., et al. 1998, Nature, 395, A14
Rodriguez, C., Taylor, G. B., Zavala, R. T., et al. 2006, ApJ, 646, 49
Salim, S., Rich, R. M., Charlot, S., et al. 2007, ApJS, 173, 267

Schlegel, D. J., Finkbeiner, D. P., & Davis, M. 1998, ApJ, 500, 525
Schneider, D. P., Richards, G. T., Hall, P. B., et al. 2010, AJ, 139, 2360
Shen, Y., Hennawi, J. F., Shankar, F., et al. 2010a, ApJ, 719, 1693
Shen, Y., Liu, X., Greene, J., & Strauss, M. 2010b, ApJ, 735, 48
Shlosman, I., Begelman, M. C., & Frank, J. 1990, Nature, 345, 679
Smirnova, A. A., Moiseev, A. V., & Afanasiev, V. L. 2010, MNRAS, 408, 400
Smith, K. L., Shields, G. A., Bonning, E. W., et al. 2010, ApJ, 716, 866
Stoughton, C., Lupton, R. H., Bernardi, M., et al. 2002, AJ, 123, 485
Strauss, M. A., Weinberg, D. H., Lupton, R. H., et al. 2002, AJ, 124, 1810
Thorne, K. S. 1987, in Three Hundred Years of Gravitation, Gravitational Radiation, ed. S. W. Hawking & W. Israel (Cambridge: Cambridge Univ. Press), 330
Toomre, A., & Toomre, J. 1972, ApJ, 178, 623
Tremonti, C. A., Heckman, T. M., Kauffmann, G., et al. 2004, ApJ, 613, 898
Tueller, J., Baumgartner, W. H., Markwardt, C. B., et al. 2010, ApJS, 186, 378
Valentijn, E. A., & Casertano, S. 1988, A&A, 206, 27
Valtonen, M. J., Lehto, H. J., Nilsson, K., et al. 2008, Nature, 452, 851
Veilleux, S., & Osterbrock, D. E. 1987, ApJS, 63, 295
Veilleux, S., Shopbell, P. L., & Miller, S. T. 2001, AJ, 121, 198
Wada, K. 2004, Coevolution of Black Holes and Galaxies (Cambridge: Cambridge Univ. Press), 186
Wang, J., Chen, Y., Hu, C., et al. 2009, ApJ, 705, L76
Wang, J., & Gao, Y. 2010, Res. Astron. Astrophys., 10, 309
White, R. L., Becker, R. H., Helfand, D. J., & Gregg, M. D. 1997, ApJ, 475, 479
York, D. G., Adelman, J., Anderson, J. E., Jr, et al. 2000, AJ, 120, 1579
Yu, Q. 2002, MNRAS, 331, 935
Yu, Q., Lu, Y., Mohayaee, R., & Colin, J. 2011, arXiv:1105.1963
Zakamska, N. L., Strauss, M. A., Krolik, J. H., et al. 2003, AJ, 126, 2125
Zakamska, N. L., Strauss, M. A., Krolik, J. H., et al. 2006, AJ, 132, 1496
Zehavi, I., Blanton, M. R., Frieman, J. A., et al. 2002, ApJ, 571, 172
Zhou, H., Wang, T., Zhang, X., Dong, X., & Li, C. 2004, ApJ, 604, L33